Imaging of Mohs Micrographic Surgery Sections Using Full-Field Optical Coherence Tomography: A Pilot Study

John R. Durkin, BS,* Jeffery L. Fine, MD,† Hakeem Sam, MD, PhD,‡
Melissa Pugliano-Mauro, MD,‡ and Jonhan Ho, MD‡

BACKGROUND Full-field optical coherence tomography (FF-OCT) is a new noninvasive imaging technique that can see down to the cellular level without tissue preparation or contrast agents.

OBJECTIVE To use FF-OCT to image Mohs micrographic surgery specimens and verify the ability of a dermatopathologist to identify or exclude malignancy.

MATERIALS AND METHODS Two Mohs surgeons supplied 18 Mohs sections from 11 patients. Each section was scanned using the FF-OCT, and a dermatopathologist blinded to the diagnosis examined the images for malignancy. The FF-OCT images were then compared with the intraoperative hematoxylin and eosin (H&E)-stained frozen sections for concordance.

RESULTS All 9 FF-OCT images interpreted as negative for malignancy were in agreement with the H&E frozen sections. Six of the remaining FF-OCT images were correctly interpreted as positive for malignancy, and three were deferred because malignancy could not be confirmed or excluded.

CONCLUSION Malignancy in Mohs sections can correctly be identified or excluded using FF-OCT. Although not ready for clinical use in its current state, FF-OCT has the potential to be incorporated into the Mohs workflow in the future.

The authors have indicated no significant interest with commercial supporter.

Mohs micrographic surgery is a surgical technique used for the complete excision of basal cell carcinoma (BCC), squamous cell carcinoma (SCC), and less commonly other types of skin cancer.[1] First described by Dr. Frederic Mohs in 1941, the original technique was termed chemosurgery because zinc chloride was used to fix tissue in vivo to allow horizontal sections to be removed and examined under the microscope.[2–4] The technique was later renamed micrographic surgery because it combines the microscopic examination of tumor margins with graphical mapping of the surgical field to allow for targeted reexcision of any remaining tumor.[5]

Current procedures no longer rely on zinc chloride for tissue fixation. Instead, the tissue is typically flattened on a glass slide, covered with an embedding medium, and placed in a cryostat for freezing. [6] This technique offers the benefit of a faster turnaround time than formalin-fixed paraffin-embedded sections, although it has its drawbacks.[7] Mohs technicians are specialists trained to prepare Mohs slides, but they are in short supply. When a Mohs technician leaves a practice, the workflow can be disrupted while a new technician is being hired. Temporary Mohs technicians used to fill open positions add significant expenses to laboratory costs. Each new technician has his or

*School of Medicine, University of Pittsburgh, Pittsburgh, Pennsylvania; †Department of Pathology, Magee-Womens Hospital of University of Pittsburgh Medical Center, Pittsburgh, Pennsylvania; ‡Department of Dermatology, University of Pittsburgh Medical Center, Pittsburgh, Pennsylvania

ISSN: 1076-0512 • Dermatol Surg 2014;40:266–274 • DOI: 10.1111/dsu.12419

her unique style that may be unfamiliar and incommodious. In addition, laboratory maintenance and reagent costs present significant ongoing expenses.[8]

Mohs surgeons are more than familiar with the ice artifact that can be a result of using a cryostat.[9] Epidermal vacuolization, splaying of collagen in the dermis, and loss of cellular architecture are all unwanted side effects of freezing the tissue.[10,11] Another disadvantage of freezing Mohs specimens is tissue shrinkage. Studies have shown that conventional Mohs slide preparation results in specimens being on average 11.6% shorter than immediately after excision.[12] This can result in uncertainty regarding the completeness of specimens. More artifacts are introduced during the cutting process, including tissue folds, which can obscure underlying tumor; transposed epidermis, which can mimic tumor in the dermis; and dark bands caused by knife chatter.[13]

After tissue fixation and sectioning, further time is needed for slide preparation and staining. Most commonly, slides are stained with hematoxylin and eosin (H&E), toluidine blue O, or safranin O.[14] Some Mohs surgeons are starting to use specialized stains such as those that stain Melan-A, AE1/AE3, and CD34.[15] The process of creating H&E frozen sections takes time and consumes precious tissue that could have otherwise been sent for further specialized staining. Improvement in the modality used to perform intraoperative analysis of Mohs sections is desirable, especially if the method is fast, is nondestructive to tissue, can be performed in vivo, parallels the spacial resolution and quality of conventional histopathology, and does not require the use of expensive Mohs technicians.

Optical coherence tomography (OCT) was first described in 1991 and since then has been applied to multiple medical fields, including dermatology.[16–19] OCT uses low-coherence interferometry to measure optical scattering from tissue, producing a two-dimensional (2D) image similar to ultrasound but with much greater resolution.[20] A more-recent variation of OCT, called full-field (FF) OCT, uses a simple halogen or light-emitting diode light source and provides 3D scans of tissue in the form of 2D slices, similar to computed tomography (CT), up to a resolution of 1.5 by 1.5 by 1 μm ($X \times Y \times Z$). The images produced using FF-OCT mimic conventional histopathology slides without tissue fixation, freezing, destruction, or staining. Tissue preparation and imaging can be performed with little training, unlike current methods. Acquisition time varies depending on the size of the tissue and desired quality of the scan, but a typical 1- by 1-cm sample can be scanned in approximately 5 minutes.[21] In addition, the digital nature of the scan is amenable to off-site evaluation or telepathology.[22]

This is the first study to use FF-OCT to create images of Mohs micrographic surgery specimens and compare them with conventional H&E-stained frozen sections.

Methods

Tissue

The experimental set-up relies on a commercially available FF-OCT system (LightCT, LLTech, Princeton, NJ) (Figure 1). Mohs samples were formalin-fixed after routine intraoperative frozen section analysis to preserve the tissues between excision and scanning. This was a practical step because formalin fixation is not necessary for FF-OCT analysis.[23] Samples were then placed in a holder with the cut surface, which was to be imaged, facing up and covered with saline. The surface to be imaged was then flattened against a silica coverslip, and a layer of silicone oil was liberally applied between the coverslip and the objective.

Image Acquisition

The light source consisted of a 150-W white halogen lamp, which provided incoherent light to illuminate the field of a 10× oil immersion microscope objec-

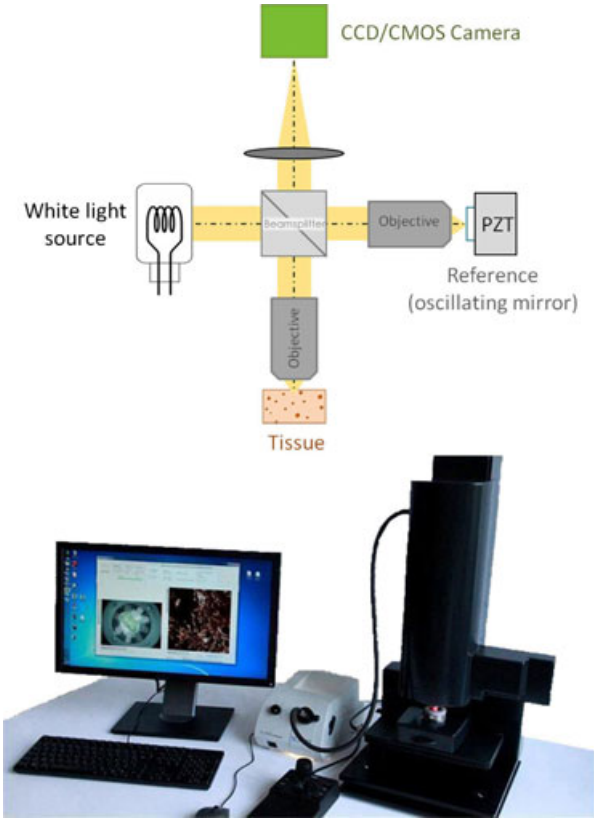

Figure 1. Full-field optical coherence tomography equipment setup.

tive over the tissue and a second objective over a reference mirror. The light reflected by the reference mirror interferes with the light reflected by the tissue, and the signal of interference is extracted using a phase-shifting method. The field of acquisition is approximate 1 mm^2. The system captures frames at approximately 69 Hz, and each image is obtained by averaging the signal over approximately 70 frames to minimize Gaussian noise. Entire tissue samples were imaged by tiling multiple image acquisitions, and image window and level were adjusted for optimal contrast.

Experimental Setup

Eighteen unique Mohs stages from 11 patients were enrolled in this study. H&E slides were obtained during the Mohs procedure using standard techniques. FF-OCT images were acquired for each tissue sample using the above methods. An honest broker de-identified each stage, which was given a case study number; that is, if a patient underwent three stages, each stage became an individual case in the study. Data sheets containing the study case number and the patient history were created. One set of data sheets was compiled with the corresponding FF-OCT images, and another duplicate set of data sheets was compiled with the corresponding glass slides. A dermatopathologist, blinded to the original diagnoses, examined the FF-OCT images and recorded the presence or absence of residual malignancy and the diagnosis (type of cancer). The dermatopathologist was permitted to defer the case if presence of a malignancy could not be determined on the FF-OCT images. Then the dermatopathologist examined the set with glass slides, blinded to the dermatopathologist's FF-OCT reads, and recorded the same data elements. Once data collection was complete, the two sets were compiled to determine concordance. If any discordance was observed, the remaining formalin-fixed tissue underwent traditional H&E processing to confirm the findings in the glass slide (Figure 2).

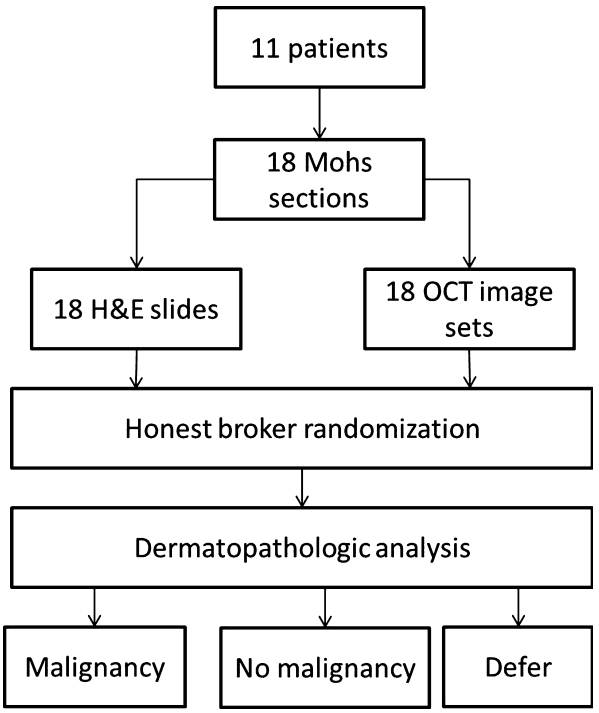

Figure 2. Experimental design.

Results

Case mix

Two Mohs surgeons supplied 11 total cases for the study; 18 stages were present in the 11 cases, but no case had more than three stages. Thirty-nine FF-OCT images were obtained. Of the 18 stages, nine were positive for malignancy, and nine were negative (Table 1). The majority of the specimens were traditional Mohs saucerizations, but a few were strips of epidermis representing a lateral margin.

Image Acquisition

Thirty-nine final FF-OCT images were used for dermatopathologic review. Images were acquired at varying depths from 0 to 80 μm, and depths were chosen to minimize artifact and capture full sections of tissue. Imaging of large specimens required dividing the image into multiple overlapping sections. Average time for a single scan of a specimen was approximately 5 to 10 minutes at the surface. Deeper scans required more signal averaging for adequate image quality and were finished in 10 to 15 minutes. A typical FF-OCT image was 13,000 by 13,000 pixels and required 240 megabytes of storage as a DICOM file and 60 megabytes of storage as a JPG file. Some difficulties encountered during scanning included getting the surface of the Mohs section to be imaged to lay flush against the glass coverplate. In addition, irregularly shaped pieces of tissue caused wasted time scanning the background because the software allowed scanning only in a rectangular region of interest.

Concordance

Of 18 diagnoses made on FF-OCT images, nine were interpreted as negative for malignancy, six were interpreted as positive for malignancy, and three were deferred. All nine interpreted as negative for malignancy on FF-OCT were confirmed as negative on glass slides, and all six interpreted as positive for malignancy were confirmed as positive on glass slides.

Normal structures were readily identified on FF-OCT images. On low magnification, epidermis was easily identified, and the FF-OCT technique accentuated the epidermal basement membrane. Sebaceous glands and adipose tissue surrounding follicles and in the subcutis were readily visualized as bright vacuolated areas. A bright basement membrane helped to outline sebaceous glands, follicles, eccrine glands, and vessels. Eccrine glands also had characteristic features and were seen as bright circular outlines arranged in clumps. Stromal collagen was recognizable as bright strands of varying thickness arranged haphazardly in the dermis (Figure 3). Fine details such as cytoplasmic contents could be visualized on high magnification.

Areas of less contrast drew immediate attention and suspicion for malignancy. On many FF-OCT images interpreted as positive for malignancy, a diagnosis could be made based merely on areas with architecture characteristic of BCC or SCC. BCCs with a nodular pattern (Figure 4), SCC in situ with a thickened epidermis, and invasive SCCs with an infiltrative pattern coupled with an epidermal

TABLE 1. Comparison of Diagnosis Between Full-Field Optical Coherence Tomography (FF-OCT) Mohs Section and Hematoxylin and Eosin (H&E)

	Diagnosis, n					
Modality	*Residual Squamous Cell Carcinoma*	*Residual Basal Cell Carcinoma*	*Residual Basosquamous Cell Carcinoma*	*No Malignancy*	*Deferred*	*Total*
FF-OCT	3	2	1	9	3	18
H&E	5	3	1	9	0	18

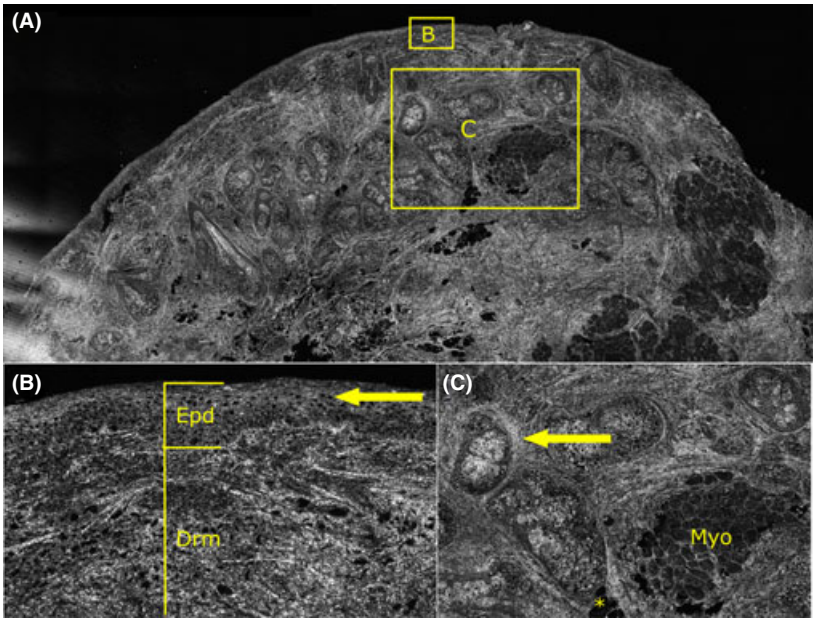

Figure 3. A representative FF-OCT Mohs section without malignancy. Epidermis is readily visualized (Epd in (B)) along with nuclei of the keratinocytes (arrow in (B)). The dermis is laden with bright, haphazardly arranged collagen fibers (Drm in (B)). The bright outlining membranes of a sebaceous gland can be seen (arrow in (C)). Myocytes appear as well defined bundle with some granularity (Myo in (C)), while adipose appear as dark globules with a mostly clear interior (asterisks in (C)).

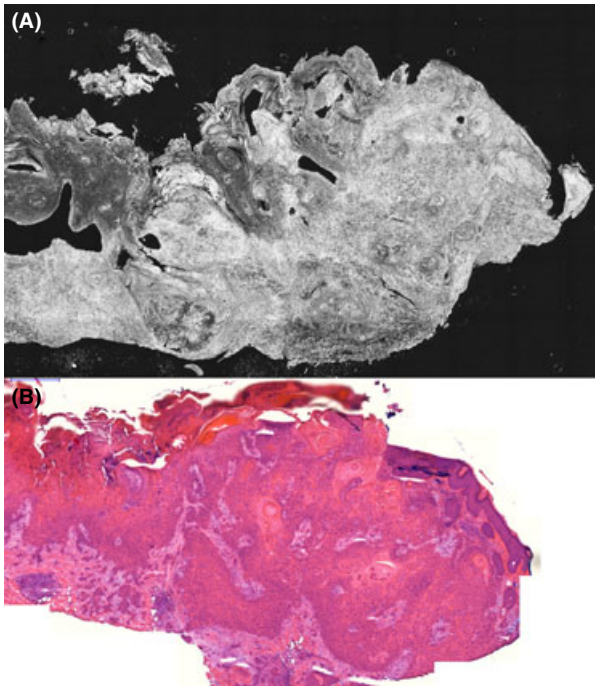

Figure 4. A basal cell carcinoma is readily seen in FF-OCT (asterisk in (A)) as well as H&E (asterisk in (B)). (Original H&E slide scanned at 40x).

connection were particularly simple to interpret (Figure 5).

Discordance

The three deferred cases were all malignant on glass slides; one was a BCC and two were SCCs. The remaining specimens from all three discordant cases were processed using formalin-fixed, paraffin-embedded procedures, and additional H&E-stained sections were obtained in case the malignancies were no longer present in the specimens scanned using FF-OCT. All three cases were confirmed to have remaining malignancies, so all three were considered to be truly discordant.

The BCC (Case 11) was a traditional Mohs saucerization specimen with a small amount of BCC with morpheaform features in the superficial and mid dermis. The carcinoma occupied approximately 2% of the entire surface area of the slide or image section. Within the dermis, there was an

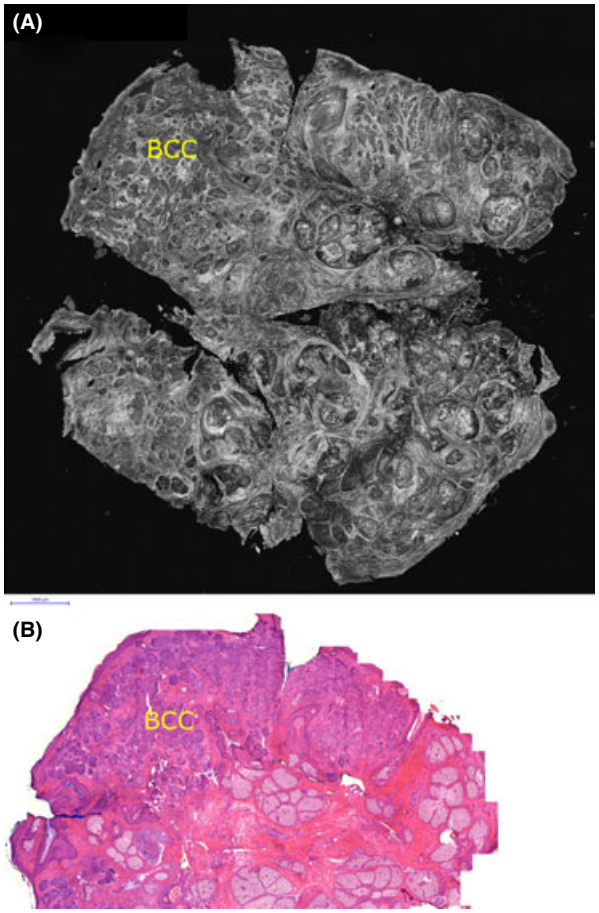

Figure 5. A squamous cell carcinoma is readily seen in FF-OCT (A) as well as H&E (B). (Original H&E slide scanned at 40×).

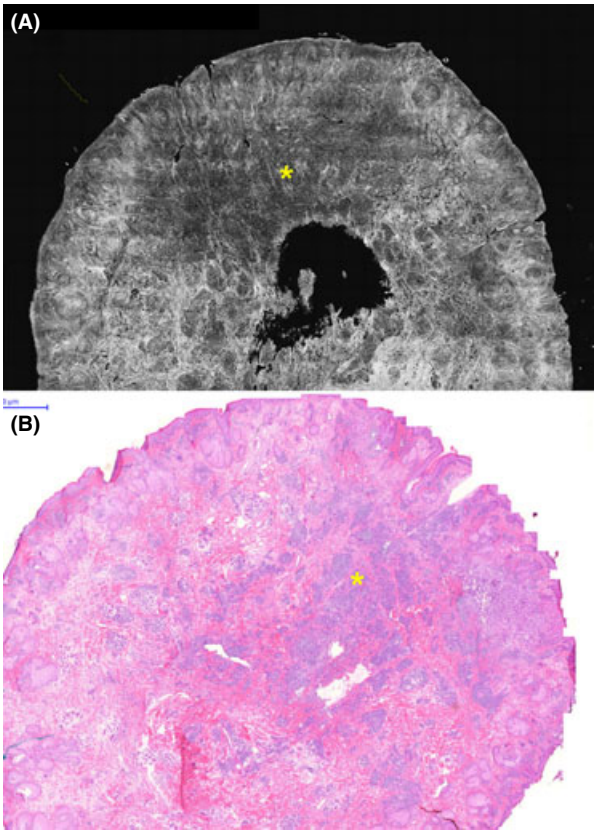

Figure 6. The basal cell carcinoma that was deferred is difficult to distinguish from surrounding inflammation on FF-OCT (A). It is more apparent with H&E (B). (Original H&E slide scanned at 40×).

exuberant accompanying lymphohistiocytic infiltrate that surrounded the carcinoma, filled the adjacent dermal stroma, and surrounded eccrine glands and vascular channels. On FF-OCT images, there was a large hypodense zone that appeared abnormal in that normal architecture was disrupted, but whether the hypodense zone represented neoplasm or inflammation could not be determined, even after direct side-by-side comparison (Figure 6). Together, the carcinoma and inflammation occupied approximately 25% of the slide or image section.

One SCC (Case 15) was a tiny focus of moderately differentiated invasive SCC located in the middermis adjacent to and underneath mature sebaceous glands. A mild adjacent lymphohistiocytic infiltrate accompanied this focus, which occupied a small percentage (~1%) of the slide or image section. Again, a hypodense focus was identified on FF-OCT (Figure 7), and although the focus was recognized as abnormal, a diagnosis of a malignancy could not be made with certainty.

The final discordant case (Case 16) was also a tiny focus of moderately differentiated SCC in the middermis surrounded by collagen and accompanied by a mild lymphohistiocytic infiltrate (Figure 8). Similar to the previous discordances, a hypodense focus was identified as abnormal, but findings were not sufficient for a definitive diagnosis of malignancy.

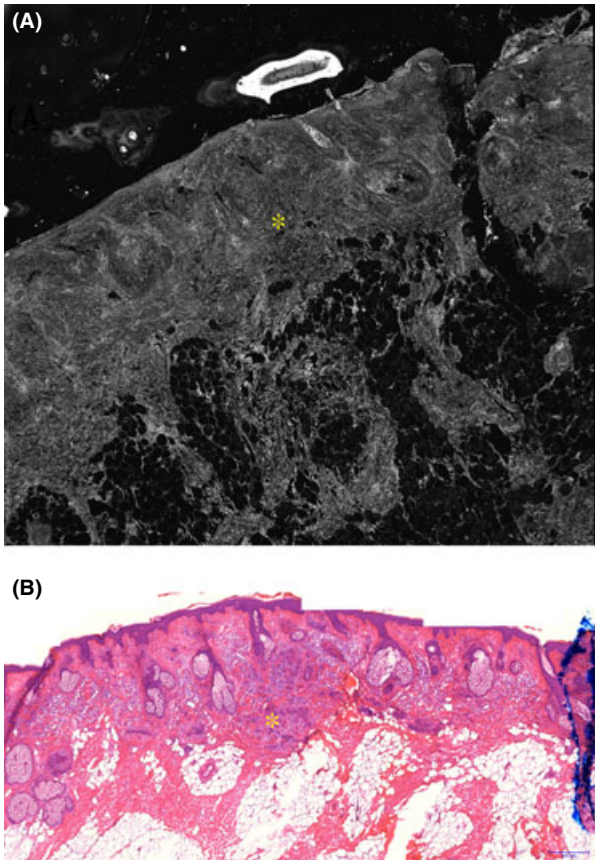

Figure 7. The first squamous cell carcinoma that was deferred can be seen as an area of hypodensity with FF-OCT (asterisk in (A)) and is readily visualized on H&E (asterisk in (B)). (Original H&E slide scanned at 40×).

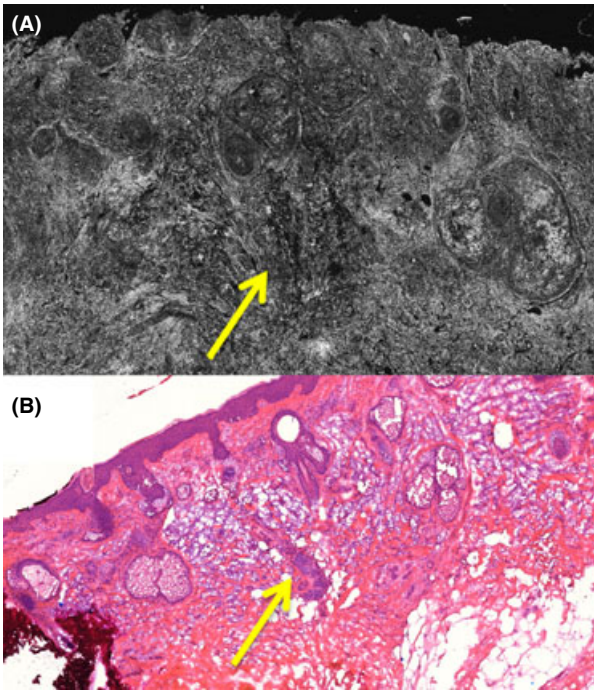

Figure 8. The second squamous cell carcinoma that was deferred can be seen as an area of hypodensity with FF-OCT (arrow in (A)) and is readily visualized on H&E (arrow in (B)). (Original H&E slide scanned at 40×).

Discussion

Image Acquisition

For FF-OCT to fit into the Mohs workflow, specimen preparation must be simpler, the machine must accommodate larger specimens, and acquisition speed needs to shorten. The chamber into which the specimen is placed does not easily accommodate the traditional Mohs saucerization specimen, which is cup-shaped and needs to be flattened to obtain a full en face section that encompasses the entire peripheral epidermis as well as the central dermis and subcutis. Flattening is easily accomplished in the frozen section workflow, but in FF-OCT, it required reducing the chamber volume by screwing the base of the chamber so it pressed the specimen against the glass surface. The more concave or convex the tissue, the more likely the periphery or the center of the specimen would not be flush against the glass surface and therefore not be imaged. We were able to compensate somewhat for curvature by imaging at multiple depths, but this is not efficient and does not allow full visualization of a true en face section. This might be alleviated by embedding the tissue in a shape-conforming material before placement in the FF-OCT chamber.

Mohs sections also tend to be large, reaching up to 2.6 cm^2 in our study, and the current specimen holder does not accommodate oversized specimens. Enlarging the sample holder and the hardware's imaging range would allow the system to accommodate larger specimens. In addition, imaging times need to be reduced to meet the demands of the Mohs workflow. Imaging time could be significantly reduced by increasing the pixel size of the sensor and, in the case of irregularly shaped specimens, by segmenting out the background and imaging only

the specimen. If this system is to be used in the Mohs workflow, it must be accommodate Mohs saucers, hold large specimens, and perform scans in much less time.

Image Interpretation and Image Quality

Although optical microscopy and FF-OCT imaging base clinical judgments on morphology, there are important differences. Whereas optical microscopy uses a primary stain and a foreground stain to examine architectural, stromal, cytologic, and nuclear details, OCT uses interference patterns to infer morphology. Architectural details are well visualized on FF-OCT images of skin. The epidermis is clearly demarcated; the direction of collagen is readily apparent; and hair follicles, sebaceous glands, and eccrine glands are well visualized. On high magnification, even some nuclear borders show striking contrast from the cytoplasm, particularly in the epidermis, but it is difficult to see individual intercellular bridges. When examining tissue for neoplasia, malignant architectural features could often be realized but were subtle, and inflamed lesions were difficult to interpret. The nodular architecture of BCCs was readily visualized, but a small focus of an infiltrative BCC, surrounded by inflammation, although it raised suspicion, could not be definitively identified in our study. The carcinoma was readily identified on H&E-stained slides. The carcinoma showed a delicate infiltrating architecture and a high nuclear cytoplasmic ratio, and the distinction from the surrounding inflammation was immediate because the inflammation did not have an architectural pattern and did not have a high nuclear to cytoplasmic ratio. Similarly, two cases with small foci of moderately differentiated SCC could not be definitively identified on FF-OCT. Even after unblinding, the findings in these areas of the FF-OCT images were subtle, although they were obvious on H&E-stained slides.

Our experience is that FF-OCT images had sufficient image quality for quick screening purposes but were limited by the reader's ability to detect small, subtle carcinomas in the dermis and carcinomas hidden within the noise of inflammation. It is likely that greater experience and better image processing techniques might alleviate some of this hesitation, but the current limitation precluding detailed examination of nuclear pleomorphism, at least in these cases, seems to be the largest aspect of the system preventing clinical use. We recognize that the field of ex vivo imaging is rapidly evolving, and perhaps the next generation of devices might capture sufficient nuclear detail.

Tissue preparation may play a role in the quality of the FFOCT images. Specimens scanned in this study were fixed in formalin to prevent tissue destruction between excision and scanning. Ideally, Mohs sections would be scanned using fresh tissue intraoperatively, but this was not possible because of the practical constraints of this study. Future studies should investigate the differences in FF-OCT image quality between formalin-fixed and fresh tissue.

One clear advantage of the FF-OCT system over optical microscopy is the possibility to develop algorithms for computer-aided diagnosis. Such algorithms are the source of intense research in radiology and could naturally be extended to these images. The system used for this study contained a package of algorithms, but exploration of the package was beyond the scope of this study. Automated image analysis identifying inflammation and fibrosis in the skin would be useful for neoplastic and inflammatory diagnoses. Automatic identification of particularly refractile cells such as eosinophils would be particularly helpful in bullous processes, drug reactions, and arthropod bites, among others. Discovering and applying a FF-OCT signature for basement membrane might help determine the invasive or in situ nature of a malignancy, and uncovering and using a signature for dermal mucin deposits might help make a diagnosis of lupus or dermatomyositis. Furthermore, if the system had the ability to obtain 3D images of large cross-sections of tissue, an alopecia examination might be done more expeditiously using

FF-OCT. The ability to visualize damaged hair follicles in three dimensions along with algorithms that could count and classify individual hair follicles, identify scarring, and categorize inflammation could go a long way toward understanding the pathophysiology of alopecia. FF-OCT has many potential applications in a wide variety of dermatologic conditions.

Conclusion

Although not ready for clinical use in its current state, FF-OCT technology shows great promise. If the current set-up better accommodated specimens, acquisition times improved, and imaging resolution advanced, the technique might become the workhorse of the Mohs surgical laboratory, potentially helping to alleviate the histotechnologist shortage and saving on reagent and capital equipment costs. Additionally, research using automated image analysis algorithms may one day extend the diagnostic toolset of Mohs surgeons and dermatopathologists.

References

1. Thomas CJ, Wood GC, Marks VJ. Mohs micrographic surgery in the treatment of rare aggressive cutaneous tumors: the Geisinger experience. Dermatol Surg 2007;33:333–9.
2. Smeets NW, Kuijpers DI, Nelemans P, Ostertag JU, et al. Mohs' micrographic surgery for treatment of basal cell carcinoma of the face—results of a retrospective study and review of the literature. Br J Dermatol 2004;151:141–7.
3. Mohs F. Chemosurgery: a microscopically controlled method of cancer excision. Arch Surg 1941;42:279–95.
4. Shriner DL, McCoy DK, Goldberg DJ, Wagner RF, et al. Mohs micrographic surgery. J Am Acad Dermatol 1998;39:79–97.
5. Gross KG, Steinman HK, Rapini RP. Mohs surgery: fundamentals and techniques. St. Louis, MO: Mosby; 1999. pp. 49–66.
6. Mikhail GR, Mohs FE. Mohs micrographic surgery. Philadelphia, PA: W.B. Saunders; 1991. pp. 13–5.
7. Vuyk HD, Lohuis PJ. Mohs micrographic surgery for facial skin cancer. Clin Otolaryngol Allied Sci 2001;26:265–73.
8. Robinson JK. Current histologic preparation methods for Mohs micrographic surgery. Dermatol Surg 2001;27:555–60.
9. Taxy JB. Frozen section and the surgical pathologist: a point of view. Arch Pathol Lab Med 2009;133:1135–8.
10. Erickson QL, Clark T, Larson K, Minsue chen T. Flash freezing of Mohs micrographic surgery tissue can minimize freeze artifact and speed slide preparation. Dermatol Surg 2011;37:503–9.
11. Rosen Y, Ahuja SC. Ice crystal distortion of formalin-fixed tissues following freezing. Am J Surg Pathol 1977;1:179–81.
12. Gardner ES, Sumner WT, Cook JL. Predictable tissue shrinkage during frozen section histopathologic processing for Mohs micrographic surgery. Dermatol Surg 2001;27:813–8.
13. Desciak EB, Maloney ME. Artifacts in frozen section preparation. Dermatol Surg 2000;26:500–4.
14. Davis DA, Pellowski DM, William hanke C. Preparation of frozen sections. Dermatol Surg 2004;30(12 Pt 1):1479–85.
15. Miller CJ, Sobanko JF, Zhu X, Nunnciato T, et al. Special stains in Mohs surgery. Dermatol Clin 2011;29:273–86, ix.
16. Huang D, Swanson EA, Lin CP, Schuman JS, et al. Optical coherence tomography. Science 1991;254:1178–81.
17. Al-mujaini A, Wali UK, Azeem S. Optical coherence tomography: clinical applications in medical practice. Oman Med J 2013;28:86–91.
18. Chen J, Lee L. Clinical applications and new developments of optical coherence tomography: an evidence-based review. Clin Exp Optom 2007;90:317–35.
19. Fujimoto JG, Pitris C, Boppart SA, Brezinski ME. Optical coherence tomography: an emerging technology for biomedical imaging and optical biopsy. Neoplasia 2000;2:9–25.
20. Sattler E, Kästle R, Welzel J. Optical coherence tomography in dermatology. J Biomed Opt 2013;18:061224.
21. Assayag O, Grieve K, Devaux B, Harms F, et al. Imaging of non-tumorous and tumorous human brain tissues with full-field optical coherence tomography. Neuroimage Clin 2013;2:549–57.
22. Cross SS, Dennis T, Start RD. Telepathology: current status and future prospects in diagnostic histopathology. Histopathology 2002;41:91–109.
23. Jain M, Shukla N, Manzoor M, Nadolny S, et al. Modified full-field optical coherence tomography: a novel tool for rapid histology of tissues. J Pathol Inform 2011;2:28.

Address correspondence and reprint requests to: John R. Durkin, BS, University of Pittsburgh School of Medicine, 3550 Terrace Street, Pittsburgh, Pennsylvania 15213, or e-mail: jrd66@pitt.edu